JOURNAL OF GUIDANCE, CONTROL, AND DYNAMICS
Vol. 27, No. 6, November–December 2004

Unpowered Approach and Landing Guidance Using Trajectory Planning

C. A. Kluever*
University of Missouri–Columbia, Columbia, Missouri 65211

A guidance scheme that employs a trajectory-planning algorithm has been developed for the approach and landing phase of an unpowered reusable launch vehicle. The trajectory-planning scheme computes a reference flight profile by piecing together several flight segments that are defined by a small set of geometric parameters. A feasible reference profile that brings the vehicle from its current state to a desired landing condition is obtained by iteration on a single geometric parameter, and the flight-path angle at the start of the flare is selected as the iteration variable. Open- and closed-loop guidance commands are readily available once the reference trajectory is obtained. The trajectory-planning algorithm is able to generate new reference profiles quickly for test cases with large variations in winds, vehicle energy, and vehicle drag. The effectiveness of the trajectory-planning algorithm is demonstrated by several numerical simulations that show that the guided vehicle is able to land successfully with an adequate energy margin.

Nomenclature

a_i = reference altitude cubic polynomial coefficients, $i = 0, 1, 2, 3$
C_D = drag coefficient
C_{D0} = zero-lift drag coefficient
C_L = lift coefficient
D = drag force, lb
g = Earth's gravitational acceleration, $= 32.174$ ft/s^2
h = altitude above runway, ft
K = lift-induced drag coefficient parameter
K_D = altitude rate error gain, g · s/ft
K_I = altitude error integral gain, g/ft · s
K_P = altitude error gain, g/ft
K_q = pitch-rate gain, rad/g · s
L = lift force, lb
M = Mach number
m = vehicle mass, slugs
n_X = vehicle acceleration along negative x-body axis, g's
n_Z = vehicle acceleration along negative z-body axis, g's
q = pitch rate, rad/s
$\bar{q}$ = dynamic pressure, lb/ft^2
R = circular pull-up radius, ft
S = vehicle reference area, ft^2
s = ground track distance for cubic altitude reference, ft
t = time, s
t_{ER} = energy reserve, s
V = ground-relative velocity magnitude, ft/s
V_∞ = freestream velocity magnitude, ft/s
x = downrange position along runway centerline, ft
α = angle of attack, rad
β = inverse scale height, ft^{-1}
γ = flight-path angle, rad
θ = vehicle pitch attitude angle, rad
ρ = atmospheric density, slugs/ft^3

Subscripts

ALI = approach and landing interface
C = center of circular pull-up arc
cmd = command
capt = steep glideslope capture point
flare = start of flare maneuver
PU = start of pull-up maneuver
ref = reference trajectory
SGS = steep glideslope
TD = touchdown
zero = downrange intersection of steep glideslope
0 = sea-level value

Received 27 January 2004; revision received 8 April 2004; accepted for publication 12 April 2004.

*Associate Professor, Mechanical and Aerospace Engineering Department, E3414 Engineering Building East. Associate Fellow AIAA.

Introduction

A MAJOR objective of NASA's second-generation reusable launch vehicle (RLV) program includes significant improvements in vehicle safety, reliability, and operation costs. A specific goal is to reduce the probability of a catastrophic failure from 1 in 500 missions (the current space shuttle goal) to 1 in 10,000 missions.[1] Hanson[1,2] has argued that advanced guidance and control (AG&C) technologies will greatly improve the overall safety and reliability of future RLV missions. In particular, AG&C methods may be able to return safely an RLV that is plagued by scenarios such as vehicle mismodeling that results in control problems, aerosurface failures, poor vehicle performance, and larger than expected flight dispersions. Advanced guidance methods have been developed for the ascent and entry phases of an RLV,[3–9] whereas advanced control methods have been developed for attitude control and control allocation.[10–13]

Approach and landing (A&L) is a critical flight phase that brings the unpowered vehicle from the terminal area energy management (TAEM) phase to runway touchdown. The space shuttle A&L guidance scheme uses a reference altitude profile that consists of an initial steep glideslope, followed by a pull-up maneuver to a shallow glideslope.[14,15] This two-phase flight-path approach has been proven to be effective for unpowered vehicles (like the shuttle) with relatively low lift-to-drag ratios (L/D). The shuttle, however, relies on a small number of fixed reference trajectories, where the nominal steep glide angle is reduced by 2 deg for heavy vehicles, and the steep glideslope is moved 1000 ft closer to the runway threshold for headwinds. Onboard trajectory generation may offer a potentially advantageous AG&C technique that can safely and reliably deliver an RLV to its landing site in the presence of extreme conditions. Schierman et al.[16] have developed a trajectory reshaping algorithm for the A&L phase of an RLV. Their algorithm interrogates a neural network that stores a database of precomputed optimal trajectories that span the expected values for the vehicle states and critical parameters (such as vehicle drag). Barton and Tragesser[17] present an automated trajectory design algorithm for the A&L phase of the

X-34, and their algorithm computes the angle and location of a steep glideslope for flight at constant dynamic pressure. Their algorithm is intended for quick (offline) computation of a new reference profile during the preliminary vehicle design stage, but may also serve as a starting point for an onboard trajectory generation scheme.

This paper presents an A&L guidance methodology that employs a trajectory-planning algorithm. The work presented in this paper differs from the work found in Refs. 16 and 17 in several ways. First, the proposed trajectory-planning method computes a feasible path from the current state to the desired touchdown state, without relying on a precomputed, stored database of neighboring A&L trajectories. Second, because the trajectory-planning algorithm computes a reference profile composed of flight paths connecting the current state to a desired touchdown state, large transient trajectory errors (such as at the beginning of A&L) are avoided. In addition, the open- and closed-loop guidance commands are readily available once the trajectory flight segments are obtained. Finally, the path-planning scheme employs approximations of the governing dynamics, and the guidance determines the entire reference geometry by iteration on a single parameter. The effectiveness of the proposed guidance algorithm is demonstrated by the simulation of A&L scenarios with winds, energy variations, and vehicle drag variations.

System Models

Equations of Motion

The unpowered RLV is considered a point mass, and its gliding motion in a vertical plane is defined by

$$\dot{V} = -D/m - g\sin\gamma \tag{1}$$

$$\dot{\gamma} = L/mV - (g/V)\cos\gamma \tag{2}$$

$$\dot{h} = V\sin\gamma \tag{3}$$

$$\dot{x} = V\cos\gamma \tag{4}$$

where lift and drag forces are defined in the usual manner

$$L = \bar{q}SC_L \tag{5}$$

$$D = \bar{q}SC_D \tag{6}$$

and dynamic pressure is $\bar{q} = \rho V^2/2$. The governing equations of motion (1–4) are with respect to a flat-Earth model, where the $+x$ axis points along the runway centerline, with the origin at the runway threshold. Atmospheric density ρ is computed with the Standard Atmosphere. Figure 1 is a free-body diagram of the point-mass RLV, and it presents the force vectors and definitions of flight-path angle, pitch attitude, and angle of attack. (Note that both γ and θ are negative in Fig. 1.)

Vehicle Models

The X-33 is the test vehicle for guidance algorithm development. This vehicle was used because much of the previous work in the AG&C program (such as entry and ascent guidance) used

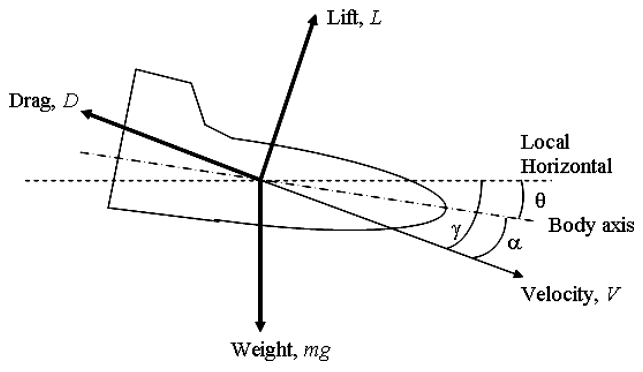

Fig. 1 Free-body diagram of the point-mass vehicle.

Table 1 Drag polar parameters for the X-33

Mach	C_{D_0}	K	N
0.3	0.0980	0.1456	2.0
0.4	0.0975	0.1819	2.2
0.5	0.0970	0.2123	2.3
0.6	0.0965	0.2311	2.3

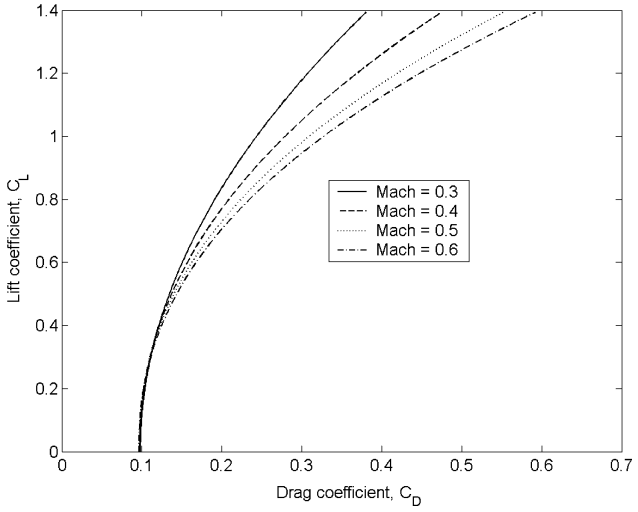

Fig. 2 Drag polar for the X-33.

the X-33, and, therefore, the vehicle parameters and aerodynamic characteristics were readily available. The true X-33 aerodynamic coefficients (required for the trajectory simulation) are computed by a two-dimensional table look-up with angle of attack and Mach number as the independent variables:

$$C_L = C_L(\alpha, M), \qquad C_D = C_D(\alpha, M) \tag{7}$$

We assume that lift and drag coefficients are the trimmed values. Incremental changes in lift and drag coefficients due to ground effects are also computed by a two-dimensional table look-up with altitude above the runway and angle of attack as the input variables. Ground effects are considered to be zero when altitude is greater than 100 ft.

The guidance algorithm requires an approximate model of the X-33 aerodynamics for onboard trajectory generation. The objective is to develop approximate aerodynamic models that require little computational effort and yet provide sufficient accuracy. A standard drag polar is used to model the X-33 aerodynamics:

$$C_D = C_{D0} + KC_L^N \tag{8}$$

Zero-lift drag coefficient C_{D0}, lift-induced drag coefficient parameter K, and exponent N are obtained by fitting the drag polar (8) to the true aerodynamic data from the two-dimensional look-up tables. Table 1 presents discrete values of the drag polar parameters at four discrete Mach numbers that span the A&L flight regime. The guidance algorithm estimates the drag coefficient by using Eq. (8) with a known value of C_L, and interpolated values of K, C_{D0}, and N, which are computed by linear interpolation among the data in Table 1 with Mach number as the independent variable. Figure 2 presents the drag polar for four Mach numbers. Both Table 1 and Fig. 2 show that C_{D0} remains essentially constant for $M \leq 0.6$.

A&L Reference Trajectory

Unlike the space shuttle A&L guidance, our proposed guidance strategy does not rely on precomputed, stored reference profiles. Instead, our guidance scheme performs onboard computation of a new reference trajectory based on available vehicle, environmental, and trajectory data. Once a reference A&L profile is computed, the guidance algorithm generates both open-loop (feedforward) and

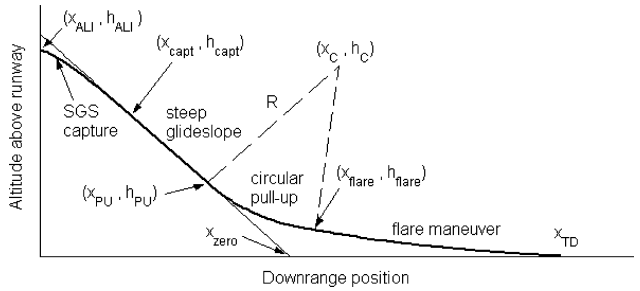

Fig. 3 Approach and landing reference trajectory geometry.

closed-loop (feedback) commands for tracking the reference trajectory. At this point, it is appropriate to discuss the details of the proposed reference trajectory geometry before discussing exactly how the reference is generated.

Figure 3 presents the various flight segments of the reference A&L trajectory, which are similar to the A&L phases of the shuttle. Several altitude profiles are pieced together with downrange position x as the independent variable. Approach and landing interface (ALI) is the transition from TAEM to A&L guidance, and this is the point where the vehicle reaches an altitude of 10,000 ft above the runway. Steep glideslope capture is the initial phase, and the RLV follows an altitude profile that eventually transitions and becomes tangent to the steep glideslope at downrange position x_{capt}. When $x \geq x_{\text{capt}}$, the steep glideslope (with constant flight-path angle) serves as the reference altitude. When the vehicle reaches the altitude h_{PU}, the pull-up guidance phase is initiated, and the RLV's velocity vector begins to rotate and the vehicle tracks a circular altitude profile that is tangent to the steep glideslope. The reference geometry transitions to the final phase, the flare maneuver, when the vehicle's downrange position reaches x_{flare}. The flare phase takes the RLV from the altitude h_{flare} to touchdown at downrange distance x_{TD}. Continuity in altitude and slope ($\mathrm{d}h/\mathrm{d}x$) are preserved between all reference flight segments.

Steep Glideslope Capture Phase

A cubic polynomial altitude profile defines the steep glideslope capture

$$h_{\text{ref}} = a_0 + a_1 s + a_2 s^2 + a_3 s^3 \tag{9}$$

where s is the ground track distance relative to ALI, that is, $s = 0$ at the initiation of A&L. The derivative of altitude with respect to ground track is the tangent of the flight-path angle:

$$\frac{\mathrm{d}h_{\text{ref}}}{\mathrm{d}s} = \tan\gamma_{\text{ref}} = a_1 + 2a_2 s + 3a_3 s^2 \tag{10}$$

Cubic polynomial coefficients a_0 and a_1 are computed from Eqs. (9) and (10) and the RLV's altitude and flight-path angle at ALI, where $s = 0$. (Note that, by definition, $h_{\text{ALI}} = 10{,}000$ ft, but γ_{ALI} may not necessarily match the steep glideslope flight-path angle.) The second- and third-order polynomial coefficients, a_2 and a_3, are also computed from Eqs. (9) and (10) with ground track distance $s = x_{\text{capt}} - x_{\text{ALI}}$ and altitude h_{capt} and flight-path angle γ_{SGS} on the steep glideslope reference (Fig. 3). Note that the shuttle A&L guidance does not utilize a separate altitude profile for transition into the steep glideslope. (The shuttle guidance immediately attempts to track the steep glideslope at initiation of the A&L phase.) Therefore, the glideslope capture phase will provide smooth transition to the steep glideslope without incurring initial transient errors. The capture altitude h_{capt} is set at a nominal value of 5000 ft, which is one-half of the altitude at ALI.

An open-loop or reference lift coefficient command can be computed directly from the reference altitude and flight-path angle profiles. To derive the required lift, we take the time derivative of $\tan\gamma_{\text{ref}}$ to obtain

$$\frac{\mathrm{d}}{\mathrm{d}t}(\tan\gamma_{\text{ref}}) = \left(1 + \tan^2\gamma_{\text{ref}}\right)\frac{\mathrm{d}\gamma}{\mathrm{d}t} \tag{11}$$

The use of the chain rule to take the time derivative of Eq. (10) yields

$$\frac{\mathrm{d}}{\mathrm{d}t}(\tan\gamma_{\text{ref}}) = \frac{\mathrm{d}}{\mathrm{d}s}(\tan\gamma_{\text{ref}})\frac{\mathrm{d}s}{\mathrm{d}t} = (2a_2 + 6a_3 s)\frac{\mathrm{d}s}{\mathrm{d}t} \tag{12}$$

Substitution of the dynamic equation for flight-path angle [Eq. (2)] and the kinematic relation for ground speed [Eq. (4)] into Eqs. (11) and (12), and setting Eq. (11) equal to Eq. (12), yields, after some algebra, the required reference lift coefficient:

$$C_L^* = [\cos\gamma_{\text{ref}}/(\bar{q}S/m)]\left[V^2(2a_2 + 6a_3 s)\cos^2\gamma_{\text{ref}} + g\right] \tag{13}$$

The vertical guidance command to the flight-control system is normal acceleration along the negative z-body axis, or n_Z, which is related to the lift and drag accelerations

$$n_Z = \frac{(L\cos\alpha + D\sin\alpha)}{mg} \tag{14}$$

Therefore, the open-loop (reference) command n_Z^* is obtained from Eq. (14), with the required lift coefficient from Eq. (13) and the corresponding drag coefficient from the drag polar (8).

Steep Glideslope Phase

The RLV maintains the constant flight-path angle (γ_{SGS}) and follows the linear altitude profile during the steep glideslope phase. Therefore, the altitude reference is simply

$$h_{\text{ref}} = \tan\gamma_{\text{SGS}}(x - x_{\text{zero}}) \tag{15}$$

where x_{zero} is the downrange location of the intersection of the steep glideslope and the ground (Fig. 3). The required lift coefficient is computed from Eq. (2) with $\dot{\gamma} = 0$:

$$C_L^* = \frac{g\cos\gamma_{\text{SGS}}}{\bar{q}S/m} \tag{16}$$

which is the same result as Eq. (13) for a linear altitude reference ($a_2 = a_3 = 0$). Open-loop reference normal acceleration is computed with Eq. (14).

Circular Pull-Up Phase

When the RLV reaches altitude h_{PU}, a circular pull-up maneuver is initiated to rotate the flight-path angle from γ_{SGS} to γ_{flare} (Fig. 3). The reference circular altitude profile is

$$h_{\text{ref}} = h_C - \sqrt{R^2 - (x - x_C)^2} \tag{17}$$

where h_C and x_C are the altitude and downrange distance to the origin of the circular pull-up arc, respectively. The required lift coefficient for the pull-up maneuver can be determined from Eq. (2) with centripetal acceleration $V\dot{\gamma} = V^2/R$

$$C_L^* = \frac{V^2/R + g\cos\gamma_{\text{ref}}}{\bar{q}S/m} \tag{18}$$

where the reference flight-path angle can be computed from the tangent line with respect to the circular arc. The reference normal acceleration command is computed with Eq. (14).

Flare Maneuver Phase

The RLV transitions to the flare maneuver when downrange $x \geq x_{\text{flare}}$. A cubic polynomial altitude profile identical to Eq. (9) defines the flare maneuver phase, and ground track distance s is measured with respect to the fixed downrange point x_{flare}, that is, $s = 0$ when $x = x_{\text{flare}}$. The four cubic polynomial coefficients are determined by specification of altitude and flight-path angle at the start of the flare, altitude and flight-path angle at touchdown ($h_{\text{TD}} = 0$), and the ground track distance of the flare maneuver, $s = x_{\text{TD}} - x_{\text{flare}}$. Equations (13) and (14) are used to compute the reference lift coefficient and reference normal acceleration, respectively, required to follow the cubic altitude profile.

Note that the shuttle A&L guidance breaks the final flight phase after the pull-up maneuver into two segments: 1) exponential decay into a shallow (constant) glideslope and 2) a final flare maneuver. Our cubic altitude flare maneuver replaces both of these segments and provides a smooth transition from the circular pull-up to desired touchdown conditions.

Trajectory Planning Algorithm

Reference trajectory planning consists of two stages: 1) steep glideslope computation and 2) backward trajectory propagation. The initial computation involves determination of the steep glideslope flight-path angle γ_{SGS}, so that the vehicle follows a quasi-equilibrium glide, where dynamic pressure is approximately constant. The desired glideslope for constant $\bar{q}$ is a function of L/D, wing loading, and initial energy. A constant-$\bar{q}$ glideslope is desirable because the vehicle can fly at a constant trim angle of attack (because C_L varies only slightly with Mach number during the A&L phase), and the states along the flight path are predictable. Once γ_{SGS} is determined, the algorithm numerically propagates a trajectory backward from the desired touchdown conditions to the start of the circular pull-up maneuver. The algorithm iterates on a single parameter (flight-path angle γ_{flare}) until the dynamic pressure at the end of the backward-propagated trajectory matches the dynamic pressure on the steep glideslope. When $\bar{q}$ matching is achieved, the trajectory-planning algorithm is finished, and the proper A&L reference profile geometry is determined. Details of the trajectory-planning algorithm are presented in the following subsections.

Quasi-Equilibrium Glideslope

Barton and Tragesser[17] have presented the quasi-equilibrium glideslope concept and its computation, and, therefore, only a summary is presented here. The objective is to determine the constant flight-path angle γ_{SGS} such that the dynamic pressure is approximately constant. To begin, take the time derivative of dynamic pressure:

$$\dot{\bar{q}} = \frac{1}{2}\frac{\mathrm{d}\rho}{\mathrm{d}h}\frac{\mathrm{d}h}{\mathrm{d}t}V^2 + \rho V\frac{\mathrm{d}V}{\mathrm{d}t} \tag{19}$$

After substitution of the kinematic relation (3) for $\mathrm{d}h/\mathrm{d}t$, and the dynamic equation (1) for $\mathrm{d}V/\mathrm{d}t$, we obtain

$$\dot{\bar{q}} = V\sin\gamma[(\rho'/\rho - \rho SC_D/m\sin\gamma)\bar{q} - \rho g] \tag{20}$$

where $\rho' = \mathrm{d}\rho/\mathrm{d}h$, which is computed from an exponential atmospheric density model

$$\frac{\mathrm{d}\rho}{\mathrm{d}h} = -\beta\rho_0\exp(-\beta h) \tag{21}$$

where the inverse scale height is $\beta = 1/30{,}499\ \mathrm{ft}^{-1}$. Therefore, the ratio ρ'/ρ in Eq. (20) is equal to $-\beta$.

The basic quasi-equilibrium glide algorithm is as follows: 1) Compute $\bar{q}$ from the airspeed and altitude at ALI. (Use this value in all subsequent calculations that involve dynamic pressure.) 2) Select a representative altitude on the steep glideslope and compute ρ. 3) Guess a trial steep glideslope angle. 4) Solve the constant flight-path angle equation [Eq. (2) with $\dot{\gamma} = 0$] for constant C_L and compute $C_D = f(C_L)$ with the drag polar. 5) Compute $\dot{\bar{q}}$ by the use of Eq. (20). 6) Adjust the steep glideslope angle by the use of the secant method until $\dot{\bar{q}} = 0$. The iterative process involves steps 4–6 until convergence is achieved. Note that a constant glideslope will not produce constant dynamic pressure because ρ changes slightly with altitude. Hence, we select a representative midpoint altitude on the steep glideslope (such as 6000 ft) and fix the atmospheric density in Eq. (20).

Note that a drag device (such as a speedbrake or split-rudder deflection) could be used to control dynamic pressure. For example, the shuttle employs a closed-loop speedbrake control channel to maintain constant equivalent airspeed (or constant $\bar{q}$) during the steep glideslope phase. However, our goal is to control dynamic pressure and touchdown for a wide range of flight conditions through trajectory reshaping and L/D modulation without reliance on a speedbrake device. The availability of a speedbrake would offer an additional degree of freedom for trajectory control and would certainly enhance the performance of our guidance design.

Trajectory Propagation and Dynamic Pressure Matching

The second major computation in the trajectory-planning algorithm is the proper selection of the flare and pull-up geometry such that backward trajectory propagation matches the dynamic pressure on the steep glideslope. First, the velocity along the flare trajectory is computed by numerical integration of $\mathrm{d}V/\mathrm{d}x$ backward from the known touchdown state to the start of the flare maneuver. The velocity differential equation $\mathrm{d}V/\mathrm{d}x$ is obtained by division of Eq. (1) by Eq. (4), and the cubic altitude profile is determined by the altitude and flight-path angle at both ends of the flare trajectory, as well as the total ground track of the flare. Flight-path angle at touchdown (γ_{TD}) can be computed from the desired touchdown speed and sink rate, and touchdown altitude is obviously zero. Therefore, altitude and flight-path angle at the start of the flare (h_{flare} and γ_{flare}) and total ground track of the flare (s_{flare}) are three potential free variables for shaping the flare maneuver, that is, shaping the cubic altitude profile. Because our goal is to design a simple guidance algorithm, we choose to fix two of these parameters and only iterate on a single free parameter. Therefore, h_{flare} is fixed at a nominal value, and the flare ground track is determined by

$$s_{\text{flare}} = \frac{3(h_{TD} - h_{\text{flare}})}{2\tan\gamma_{TD} + \tan\gamma_{\text{flare}}} \tag{22}$$

Equation (22) is the maximum total ground track for a cubic altitude profile with a monotonically increasing flight-path angle, and this expression can be derived from Eqs. (9) and (10). If the flare ground track is greater than s_{flare} in Eq. (22), the flight-path angle during the flare will reach a value greater than γ_{TD}, which will result in an unnecessary flight-path modulation and excessive speed loss during the flare. Velocity during the flare is controlled by proper selection of the single free parameter, γ_{flare}; this parameter determines the initial slope of the cubic altitude profile and the total ground track via Eq. (22). Drag coefficient is required for numerical integration of $\mathrm{d}V/\mathrm{d}x$, and C_D is computed from the drag polar (8) with the lift coefficient required to follow the cubic reference [see Eq. (13)]. A low-order (second/third) Runge–Kutta method is used to integrate the single differential equation numerically to reduce the computational load of the guidance algorithm.

Backward integration of the circular pull-up maneuver is computed via the end state from backward integration of the flare. Velocity information is obtained by integration of $\mathrm{d}V/\mathrm{d}\gamma$ backward from γ_{flare} to γ_{SGS}. The velocity differential equation is obtained by division of Eq. (1) by Eq. (2). Numerical integration of $\mathrm{d}V/\mathrm{d}\gamma$ requires both lift and drag coefficients, and C_L is computed from Eq. (18) and C_D from the drag polar (8). The low-order Runge–Kutta method is used to perform the numerical integration. The appropriate pull-up radius R is determined from Eq. (18) with the velocity, flight-path angle, lift coefficient, and dynamic pressure from the start of flare maneuver, that is, the transitional point between pull-up and flare. The solution of the appropriate radius ensures continuity in normal acceleration (and, hence, angle of attack) as the RLV transitions from pull-up to flare maneuver. The dynamic pressure is computed from the end state from the backward pull-up integration, that is, the end of the steep glideslope, and this value is compared with $\bar{q}$ from the quasi-equilibrium steep glideslope. The two-segment backward propagation process is repeated by iteration on γ_{flare} until the propagated dynamic pressure matches the steep glideslope dynamic pressure. (The secant method is used for the iteration process.)

Our subsequent numerical simulations demonstrate that the two-segment iteration scheme is able to converge to the appropriate value for γ_{flare} in all test cases. However, an operational algorithm will require a safeguard against a divergent search process that has not converged in a timely manner. One possible backup method is to switch from the secant search to a scheme that simply propagates

N additional backward trajectories for a fixed range of γ_{flare} values and then selects the flight-path angle that results in the minimum absolute error in dynamic pressure.

Note that the flare geometry (h_{flare}, γ_{flare}, s_{flare}, and x_{TD}), pull-up radius R, and steep glideslope γ_{SGS} completely define the remaining reference profile parameters, such as pull-up altitude and downrange distance (h_{PU} and x_{PU}), circular arc center coordinates (h_C and x_C), and steep glideslope intersection point (x_{zero}). Furthermore, dramatic changes in aerodynamic properties, wing loading, wind conditions, or initial energy will cause the trajectory-planning algorithm to alter the reference profile, which will include shifting the steep glideslope either closer to or farther from the runway. Hence, the steep glideslope capture phase provides a smooth transition without incurring large altitude errors at the initiation of A&L.

A&L Simulation

Normal Acceleration Command from Guidance

The total normal acceleration command $\bar{n}_Z$ is the sum of open-loop and closed-loop normal acceleration commands:

$$\bar{n}_Z = n_Z^* + \Delta n_Z \tag{23}$$

The open-loop or reference command (n_Z^*) is computed via Eq. (14) and the lift coefficient required to follow the respective reference trajectory segment [Eqs. (13), (16), or (18)]. A simple proportional–integral–derivative (PID) scheme is used for closed-loop control:

$$\Delta n_Z = K_P \Delta h + K_I \int \Delta h \, \mathrm{d}t + K_D \Delta \dot{h} \tag{24}$$

where $\Delta h = h_{\text{ref}} - h$ and $\Delta \dot{h} = \dot{h}_{\text{ref}} - \dot{h}$. A constant set of PID gains is used throughout A&L, with the exception that integral control is used only during the steep glideslope and circular pull-up phases. The PID gains used here are $K_P = 0.003$ g/ft, $K_I = 0.00016$ g/ft · s, and $K_D = 0.015$ g · s/ft. These values are similar to the shuttle gains, which also use a 5:1 ratio between the rate and proportional gains.[14]

Numerical Simulation

Simulink® is used to assess the proposed guidance scheme, and Fig. 4 presents a simplified block diagram of the closed-loop simulation. Because the truth aerodynamic two-dimensional tables require angle-of-attack as an input, the longitudinal pitching motion must be modeled in some fashion. The guidance algorithm generates the total normal acceleration command every 0.1 s (10 Hz), which is differenced with the actual normal acceleration of the RLV, and the error is sent to the flight-control system. A pitch-rate command proportional to normal acceleration error is generated

$$q_{\text{cmd}} = K_q(\bar{n}_Z - n_Z) \tag{25}$$

where $K_q = 0.7$ rad/g · s is the pitch-rate gain. A simple unity-gain, first-order lag model approximates pitch-rate response:

$$\dot{q} + 2q = 2q_{\text{cmd}} \tag{26}$$

Equation (26) approximates the coupling of the pitch dynamics and the closed-loop flight-control system, and it assumes that the inner-loop pitch channel is fast, well damped, and accurate with zero steady-state error. Pitch rate is then integrated, and angle-of-attack is determined from the difference between pitch attitude and flight-path angles ($\alpha = \theta - \gamma$). Numerical integration of the point-mass dynamics [Eqs. (1–4)] is performed by a Runge–Kutta method with a fixed time step of 0.1 s.

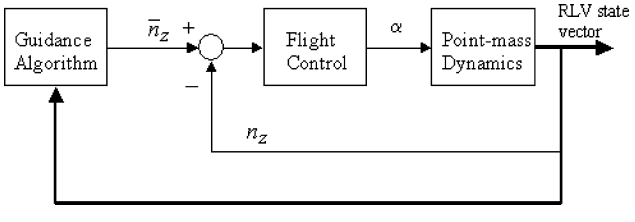

Fig. 4 Simplified approach and landing block diagram.

Numerical Results

Nominal Approach and Landing Trajectory

A baseline approach and landing trajectory is obtained by execution of the simulation with the nominal ALI state, no winds, and nominal RLV aerodynamics. The nominal ALI state is $h_{\text{ALI}} = 10{,}000$ ft (by definition) and $V_{\text{ALI}} = 570$ ft/s (Mach 0.54). Michaels Army Air Field is the landing site (altitude above sea level is 4340 ft), and, therefore, the initial dynamic pressure is 248.2 psf. The desired touchdown conditions are $V_{\text{TD}} = 306$ ft/s, $\dot{h}_{\text{TD}} = -3$ ft/s, and $x_{\text{TD}} = 1400$ ft. The path-planning algorithm was executed offline before running the simulation, and both the quasi-equilibrium glideslope computation and the backward trajectory propagation converged in seven iterations. Flight-path angle and downrange distance at ALI for the nominal A&L profile were determined to be $\gamma_{\text{ALI}} = -25.24$ deg and $x_{\text{ALI}} = -26{,}316$ ft, respectively. Table 2 lists the reference trajectory parameters as computed by the planning algorithm for nominal flight conditions. Note that for nominal conditions, the steep glideslope capture phase is essentially reduced to the steep glideslope profile because the nominal ALI point begins on the steep glideslope with the proper flight-path angle.

Figures 5 and 6 present the nominal A&L trajectory obtained from execution of the Simulink model. Figure 5 shows that equivalent airspeed (or $\bar{q}$) is essentially constant during the steep glideslope ($t < 34$ s), as predicted by the quasi-equilibrium glide condition. The guidance algorithm demonstrates good tracking performance; altitude error never exceeds 5 ft and flight-path angle error remains less than 0.3 deg. The largest transient errors occur when the circular

Table 2 Reference path parameters for nominal conditions

Parameter	Nominal value
γ_{SGS}	−25.24 deg
γ_{flare}	−5.78 deg
x_{ALI}	−26,316 ft
x_{zero}	−5,100 ft
x_{PU}	−9,847 ft
x_{flare}	−2,324 ft
x_C	4.2 ft
x_{TD}	1,400 ft
h_{ALI}	10,000 ft
h_{PU}	2,238 ft
h_C	23,141 ft
h_{flare}	150 ft
R	23,108 ft

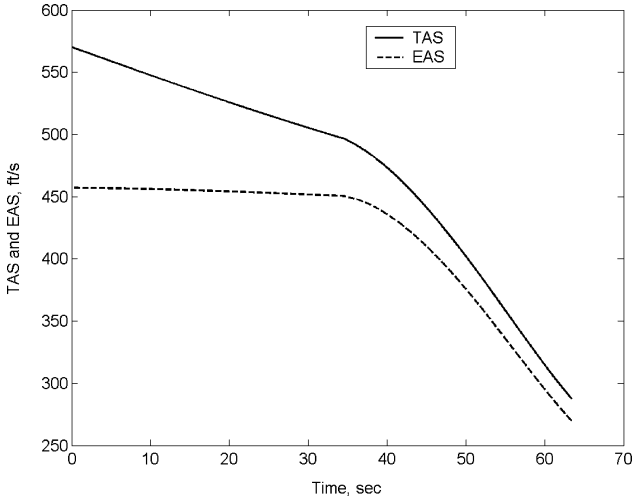

Fig. 5 True airspeed and equivalent airspeed for a nominal approach and landing.

Table 3 Trials with winds and energy variations

Wind conditions	γ_{SGS}, deg	x_{zero}, ft	R, ft	V_∞(TD), ft/s	$\dot{h}_{TD}$, ft/s	$\bar{q}_{TD}$, psf	x_{TD}, ft	θ_{TD}, deg	t_{ER}, s
No winds	−25.2	−5100	23,108	287.3	−2.8	86.3	1,671	7.7	8.3
28-kn headwind[a]	−25.2	−5100	23,108	222.4	−2.4	51.7	1,776	14.2	0.0
28-kn tailwind[a]	−25.2	−5100	23,108	328.0	−3.7	112.4	1,586	5.6	11.5
28-kn headwind[b]	−23.2	−1577	9,709	305.7	−1.7	97.6	1,475	6.9	9.9
28-kn tailwind[b]	−27.4	−9717	39,558	274.8	−3.2	78.9	1,638	8.3	7.1

[a]Path-planning algorithm is not used (use nominal reference trajectory). [b]Path-planning algorithm is executed at ALI (compute new reference trajectory).

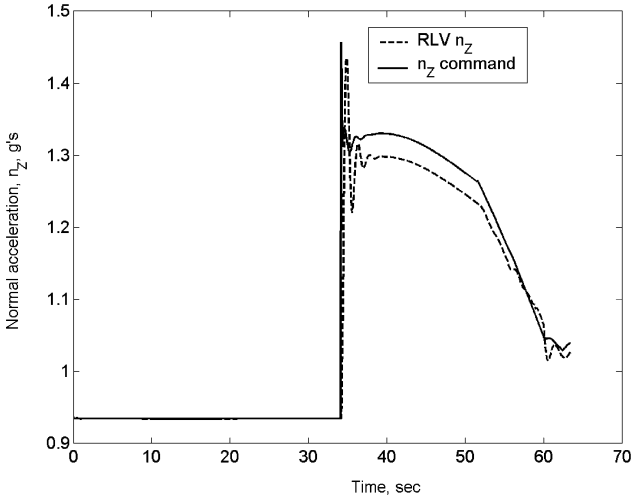

Fig. 6 Normal acceleration for a nominal approach and landing.

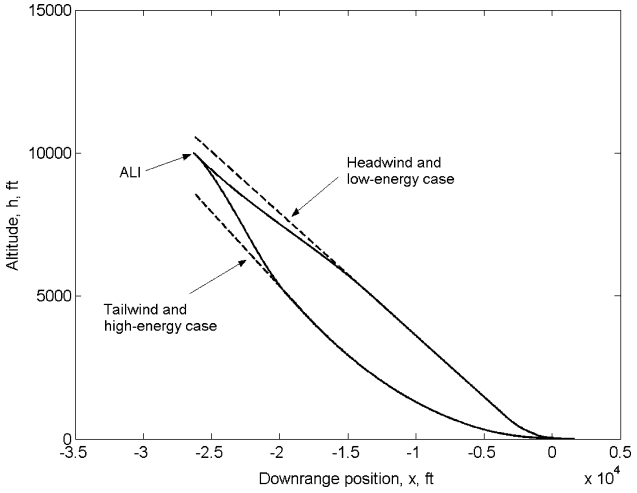

Fig. 7 Altitude profiles for headwind and tailwind cases: ——, RLV altitude and - - - - -, steep glideslope.

pull-up is initiated ($t = 34$ s), but these errors are quickly damped out. Figure 6 presents normal acceleration along with the guidance command. Load factor is constant during the steep glideslope, and the step command at 34 s initiates the circular pull-up. Note that the normal acceleration command is continuous as the circular pull-up transitions to the flare maneuver ($t = 52$ s) due to the proper computation of the pull-up radius. The touchdown speed from the nominal simulation is 287 ft/s, and the touchdown sink rate is 2.8 ft/s. The RLV lands at a downrange distance of 1671 ft, which is 271 ft beyond the desired touchdown location. Consequently, the touchdown speed is slightly lower than the nominal value due to an extra second in flight.

Trials with Winds and Energy Variation

The first test cases involve landing in high winds with high- and low-energy conditions. It is assumed that estimates of the wind speed components are available to the path-planning algorithm. Therefore, the path-planning scheme estimates the true airspeed (V_∞) by subtracting the wind speed component from the known ground speed and uses V_∞ to compute the dynamic pressure for the quasi-equilibrium glide and backward trajectory propagation. In the best-case scenario, the path-planning scheme will receive low-altitude wind information during the TAEM phase and recompute a new A&L reference trajectory and corresponding ALI target. Therefore, a closed-loop TAEM guidance scheme could conceivably deliver the RLV to this updated ALI point, and the A&L phase would proceed with little deviation from the updated reference path that has accounted for winds. In the worst-case scenario, TAEM would deliver the RLV to the nominal ALI point, and the vehicle would initially acquire wind information as the A&L phase begins. (This extreme scenario pertains to either sudden winds at 10,000 ft, or a complete lack of low-altitude wind information during the TAEM phase.) We will test the path-planning algorithm under the worst-case scenario with a constant downrange wind speed of 50 ft/s (28.4 kn). We also assume that V_∞ at ALI is off the nominal value by 30 ft/s in the worst direction; therefore, true airspeed is 540 ft/s (low energy) for a headwind, and true airspeed is 600 ft/s (high energy) for a tailwind.

Table 3 presents the touchdown conditions from simulations with winds and initial energy variation (the no-wind nominal case is shown for comparison). For the first two cases with winds, the path-planning algorithm is not engaged, and the RLV uses the fixed reference profile from the nominal (no-wind) scenario. (Note that the reference path parameters are static.) The RLV is initially on the nominal profile at ALI, and, therefore, zero trajectory errors exist at the start of A&L for these two cases. Energy reserve t_{ER} (final column in Table 3) is defined in Ref. 14 as the time required for deceleration from touchdown airspeed to stall speed, given constant drag deceleration. The minimum energy reserve design requirement is 5 s for the space shuttle.[14] Stall speed of the X-33, which is computed under the assumption of a 15-deg maximum angle of attack at landing, is 222.1 ft/s. The two cases without the path-planning algorithm track the static reference profile very well, but the airspeed at touchdown is either quite small (headwind) or large (tailwind). For the headwind case, the RLV essentially lands at the stall speed, and, hence, the energy reserve is zero. In addition, pitch attitude is large for the headwind case, and the RLV may be close to tailscrape at landing.

The same two headwind and tailwind cases were rerun with the trajectory-planning algorithm engaged, and the results are shown in the last two rows of Table 3. Note that the location of the steep glideslope changes significantly with the wind direction and that glideslope angle is only slightly adjusted. Furthermore, the pull-up radius is significantly reduced for the headwind (low-energy) case and significantly increased for the tailwind (high-energy) case. The RLV's initial altitude and flight-path angle are different from the corresponding reference values at the same downrange location. (Recall that we have fixed the initial states to the nominal ALI values: $\gamma_{ALI} = -25.2$ deg; $h_{ALI} = 10{,}000$ ft; and $x_{ALI} = -26{,}316$ ft.) Hence, the steep glideslope capture phase plays an important role. Figure 7 presents the altitude profiles for both the headwind and tailwind cases, and the significant changes in the reference profiles are evident. Both cases with the trajectory-planning algorithm resulted in successful landings, with touchdown airspeeds near the nominal value and sufficient energy reserve.

Trials with Drag Variation

Next, a series of simulations with vehicle drag variations was obtained. Drag variations may be due to mismodeled aerodynamics (relatively small variations) and control surface failures (large variations). For example, a failed or damaged control surface might result in excessive trim drag, which is caused by a reconfigurable inner-loop control law that is required to maintain rotational equilibrium. Recall that the trajectory-planning algorithm and open-loop guidance command rely on an approximate aerodynamic model (the drag polar). We assume that the vehicle is able to estimate its aerodynamic performance based on accelerometer measurements along the negative x and z body axes:

$$\frac{1}{mg}\begin{bmatrix} L \\ D \end{bmatrix} = \begin{bmatrix} \cos\alpha & -\sin\alpha \\ \sin\alpha & \cos\alpha \end{bmatrix}\begin{bmatrix} n_Z \\ n_X \end{bmatrix} \tag{27}$$

Estimation of lift and drag forces in real time is complicated by noisy accelerometer measurements, difficulty in measurement of dynamic pressure, and time-varying control deflections. In this study, we assume that perfect knowledge of vehicle lift and drag is available. Hence, the proposed guidance algorithm could periodically compare the lift and drag estimates with the drag polar model and recompute the reference A&L trajectory if the deviations become large. If aerodynamic variations are observed early in the TAEM phase, then the trajectory-planning algorithm can recompute the ALI target, and the closed-loop TAEM guidance will attempt to deliver the RLV to this new target point. A far worse situation involves a sudden change in vehicle drag at the start of A&L, when the RLV is assumed to be on (or near) the nominal ALI point. In this scenario, the vehicle may not be able to land successfully by using a fixed A&L reference profile that was computed with the nominal aerodynamic model.

Table 4 presents the touchdown conditions from six simulations with drag variation. (The nominal drag case is shown for comparison.) In all cases, the reference profile is fixed via the parameters summarized in Table 2 (the reference trajectory with nominal aerodynamics). The RLV is initially on the nominal profile at ALI, and, therefore, zero trajectory errors exist at the start of A&L. For each trial, vehicle drag coefficient is increased or decreased in increments of 10% of its nominal value throughout the trajectory. Table 4 shows that following a static reference path with reduced drag results in acceptable sink rates at touchdown; however, the touchdown speed becomes quite large as drag decreases. Increasing drag causes low-energy conditions when the RLV is forced to follow the static reference path, and, subsequently, the touchdown speed decreases as drag increases. Energy reserve is less than the 5-s shuttle requirement for all cases with increased drag, and the 20 and 30% drag cases result in touchdown speeds less than stall speed. A 20% increase in drag results in an acceptable sink rate (5.8 ft/s), but the pitch angle at touchdown (18.7 deg) would probably result in tail-scrape. The case with 30% increase in drag does not land successfully.

Table 4 Drag variation trials with a fixed reference trajectory

ΔC_D, %	V_{TD}, ft/s	$\dot{h}_{TD}$, ft/s	$\bar{q}_{TD}$, psf	x_{TD}, ft	θ_{TD}, deg	t_{ER}, s
0 (nominal)	287.3	−2.8	86.3	1671	7.7	8.3
−10	321.9	−3.1	108.2	1752	6.1	12.1
−20	352.5	−3.2	129.8	1792	5.1	15.0
−30	380.2	−3.4	151.0	1828	4.4	17.4
+10	246.5	−2.6	63.5	1522	10.5	3.1
+20	205.9	−5.8	44.3	854	18.7	−1.6
+30	193.9	−46.2	39.3	−1137	56.2	−1.0

Next, the six cases with drag variations were rerun with the trajectory-planning algorithm enabled. It is assumed that the trajectory-planning scheme has perfect knowledge of the drag variations, and adjusts C_D computed from the drag polar model. (Operationally, we envision engaging the trajectory-planning algorithm when the estimated drag shows a large mismatch with the nominal drag polar model, and in this paper we only consider the case where the drag dispersion occurs at the start of A&L.) Table 5 summarizes the six drag-variation trials with trajectory planning. (The nominal drag case is again shown for comparison.) The important reference trajectory parameters (such as steep glideslope) are also presented in Table 5. Note that the angle and location of the steep glideslope changes significantly with the drag variation: decreased drag (increased L/D) results in a shallower initial glideslope that is farther from the runway, and increased drag has the opposite effect. Therefore, the RLV's altitude and flight-path angle at ALI are quite different from the corresponding reference values at the same downrange location. (Recall that we have fixed the initial states to the nominal ALI values: $V_{ALI} = 570$ ft/s; $\gamma_{ALI} = -25.2$ deg; $h_{ALI} = 10{,}000$ ft; and $x_{ALI} = -26{,}316$ ft.) Hence the steep glideslope capture phase plays an important role. All drag variation trials shown in Table 5 result in successful landings with touchdown speeds, sink-rates, and touchdown locations near their respective nominal values. Tailscrape does not occur, and all cases meet the 5-s energy reserve criteria.

Figures 8 and 9 present the altitude and flight-path angle profiles for the extreme case where drag is increased by 30%. The glideslope capture phase plays the crucial role of smooth transition to a steeper glideslope ($\gamma_{SGS} = -37$ deg) that has been shifted closer to the runway. Figures 8 and 9 demonstrate how the RLV must initially pull up to close in on the retargeted steep glideslope, and then pull down to acquire the glideslope and maintain airspeed. The RLV cannot simply follow the initial (nominal) flight path of −25 deg because of the increased drag and subsequent loss of airspeed. Therefore, the glideslope capture phase is needed to ensure proper touchdown conditions. Figure 10 presents the normal acceleration profile for this extreme case, and several step commands and subsequent transient responses are apparent. The largest load factors are experienced during the initial 2-g pull-up for glideslope capture and the 1.8-g circular pull-up maneuver.

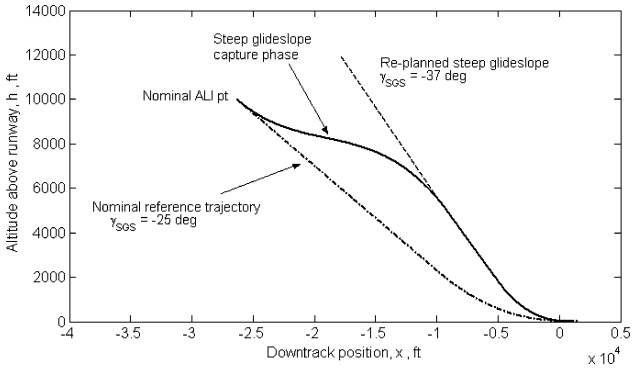

Fig. 8 Altitude profile for case with 30% increase in drag.

Table 5 Drag variation trials with trajectory-planning algorithm

ΔC_D, %	γ_{SGS}, deg	x_{zero}, ft	R, ft	V_{TD}, ft/s	$\dot{h}_{TD}$, ft/s	$\bar{q}_{TD}$, psf	x_{TD}, ft	θ_{TD}, deg	t_{ER}, s
0 (nominal)	−25.2	−5,100	23,108	287.3	−2.8	86.3	1,671	7.7	8.3
−10	−22.9	−5,756	28,560	301.6	−2.9	95.0	1,801	7.0	10.5
−20	−20.9	−6,431	34,773	314.6	−3.0	103.4	1,918	6.4	12.7
−30	−19.2	−7,389	43,335	322.0	−3.0	108.3	2,031	6.1	14.3
+10	−28.2	−4,227	17,486	281.6	−2.8	82.9	1,496	8.0	7.0
+20	−32.0	−3,573	13,376	273.7	−2.8	78.3	1,278	8.5	5.5
+30	−37.0	−2,579	8,942	283.3	−4.8	83.9	833	8.2	5.3

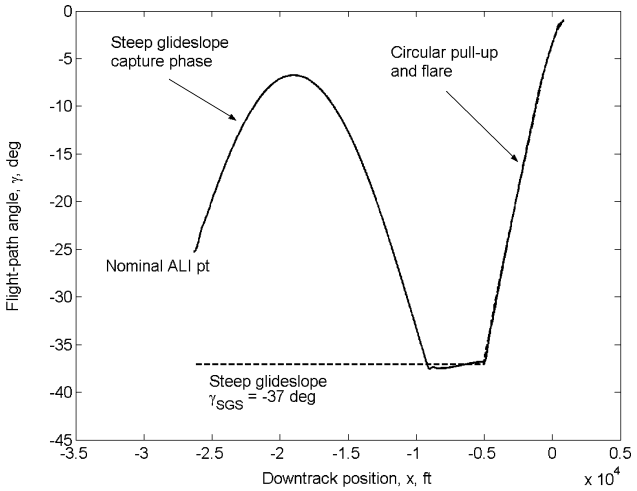

Fig. 9 Flight-path angle profile for case with 30% increase in drag.

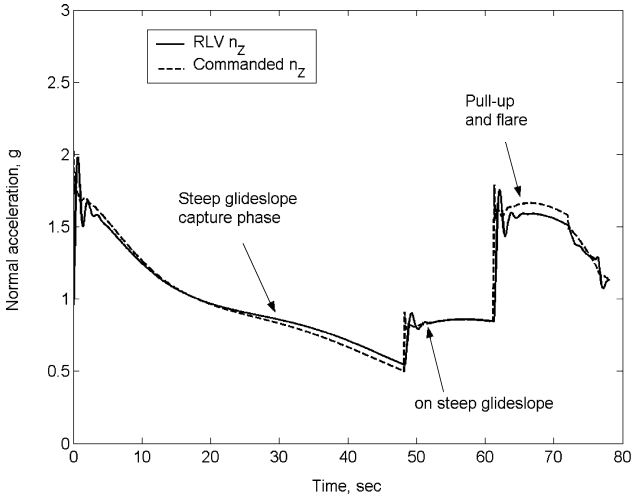

Fig. 10 Normal acceleration for case with 30% increase in drag.

Conclusions

A new guidance scheme has been developed for the approach and landing phase of an unpowered RLV. The guidance method employs a trajectory-planning algorithm that generates the reference path based on wind conditions, the energy state, and the vehicle's aerodynamic performance. The path-planning algorithm consists of a two-stage process: an iterative scheme determines the quasi-equilibrium glideslope for constant dynamic pressure and a backward trajectory-propagation scheme adjusts the flare geometry such that dynamic pressure matching at the pull-up altitude is achieved. Both subphases involve adjustment of a single free parameter, and the subsequent algorithm is robust and achieves convergence in fewer than eight iterations for all test cases.

Several closed-loop simulations were conducted to demonstrate the proposed guidance algorithm. Worst-case scenarios involving severe winds, energy variations, and vehicle drag variations were simulated, and the results show that the trajectory-planning guidance method achieved successful landings with adequate energy margins at touchdown for all cases. Furthermore, many of the extreme cases required drastic changes in the reference profile (such as large changes in the steep glide path's angle and downrange position and large changes in the circular pull-up radius); however, these dramatic changes seem to be necessary to accomplish satisfactory touchdown conditions. Touchdown conditions either deteriorated or severely violated constraints when the worst-case scenarios were simulated without the trajectory-planning algorithm and the guidance tracked a fixed (nominal) reference profile. Based on these analyses, the trajectory-planning guidance algorithm is a viable candidate for onboard implementation to improve safety and reliability of future RLVs.

Acknowledgments

This research was supported by NASA Marshall Space Flight Center under Grant NAG8-1913. The author thanks John Hanson, G. Dukeman, and J. Mulqueen for their suggestions and help.

References

[1]Hanson, J. M., "A Plan for Advanced Guidance and Control Technology for 2nd Generation Reusable Launch Vehicles," AIAA Paper 2002-4557, Aug. 2002.

[2]Hanson, J. M., "New Guidance for New Launch Vehicles," *Aerospace America*, Vol. 41, No. 3, 2003, pp. 36–41.

[3]Dukeman, G. A., "Atmospheric Ascent Guidance for Rocket-Powered Launch Vehicles," AIAA Paper 2002-4559, Aug. 2002.

[4]Sun, H., and Lu, P., "Closed-Loop Endoatmospheric Ascent Guidance," AIAA Paper 2002-4558, Aug. 2002.

[5]Calise, A., and Brandt, N., "Generation of Launch Vehicle Abort Trajectories Using a Hybrid Optimization Method," AIAA Paper 2002-4560, Aug. 2002.

[6]Dukeman, G. A., "Profile-Following Entry Guidance Using Linear Quadratic Regulator Theory," AIAA Paper 2002-4457, Aug. 2002.

[7]Zimmerman, C., Dukeman, G., and Hanson, J., "Automated Method to Compute Orbital Reentry Trajectories with Heating Constraints," *Journal of Guidance, Control, and Dynamics*, Vol. 26, No. 4, 2003, pp. 523–529.

[8]Shen, Z., and Lu, P., "Onboard Generation of Three-Dimensional Constrained Entry Trajectories," *Journal of Guidance, Control, and Dynamics*, Vol. 26, No. 1, 2003, pp. 111–121.

[9]Chen, D. T., Saraf, A., Leavitt, J. A., and Mease, K. D., "Performance of Evolved Acceleration Guidance Logic for Entry (EAGLE)," AIAA Paper 2002-4456, Aug. 2002.

[10]Shtessel, Y., Zhu, J., and Daniels, D., "Reusable Launch Vehicle Attitude Control Using a Time-Varying Sliding Mode Control Technique," AIAA Paper 2002-4779, Aug. 2002.

[11]Hodel, A. S., and Callahan, R., "Autonomous Reconfigurable Control Allocation (ARCA) for Reusable Launch Vehicles," AIAA Paper 2002-4777, Aug. 2002.

[12]Doman, D. B., and Ngo, A. D., "Dynamic Inversion-Based Adaptive/Reconfigurable Control of the X-33 on Ascent," *Journal of Guidance, Control, and Dynamics*, Vol. 25, No. 2, 2002, pp. 275–284.

[13]Johnson, E. N., and Calise, A. J., "Limited Authority Adaptive Flight Control for Reusable Launch Vehicles," *Journal of Guidance, Control, and Dynamics*, Vol. 26, No. 6, 2003, pp. 906–913.

[14]Tsikalas, G. M., "Space Shuttle Autoland Design," AIAA Paper 82-1604-CP, Aug. 1982.

[15]Walyus, K. D., and Dalton, C., "Approach and Landing Simulator for Space Shuttle Orbiter Touchdown Conditions," *Journal of Spacecraft and Rockets*, Vol. 28, No. 4, 1991, pp. 478–485.

[16]Schierman, J. D., Hull, J. R., and Ward, D. G., "Adaptive Guidance with Trajectory Reshaping for Reusable Launch Vehicles," AIAA Paper 2002-4458, Aug. 2002.

[17]Barton, G. H., and Tragesser, S. G., "Autolanding Trajectory Design for the X-34," AIAA Paper 99-4161, Aug. 1999.